Progress in Fractional Differentiation and Applications
An International Journal

http://dx.doi.org/10.18576/pfda/050202

Fractional Control of a 7-DOF Robot to Behave Like a Human Arm

André Ventura[1], *Inés Tejado*[2], *Duarte Valério*[1,*] *and Jorge Martins*[1]

[1] IDMEC, Instituto Superior Técnico, Universidade de Lisboa, Lisboa, Portugal
[2] Industrial Engineering School, University of Extremadura, Badajoz, Spain

Received: 3 Apr. 2018, Revised: 26 Jun. 2018, Accepted: 2 Jul. 2018
Published online: Apr. 2019

Abstract: Endowing robots with the ability to closely collaborate with humans is an important challenge of robotics. For this purpose, systems are required that behave in a manner humans are comfortable with, and mimicking the way another human would behave is a good choice. This paper presents simulation results of how a KUKA LWR IV robot with 7 degrees of freedom (DOF) can be made to behave like a human arm, having surgical (e.g. orthopedic) applications in view. This performance is achieved using a fractional order transfer function model of the arm, which have been presented in previous papers. Results are satisfactory and could not be obtained using only the control features provided with the robot.

Keywords: Human arm, surgical robotics, fractional control.

1 Introduction

Robots that appear and perform like humans are being developed in many fields. It is possible to identify in recent literature two main lines of research, both of similar importance to achieve behaviour truly human-like. This is because two different points of view for the problem of human-robot cooperation can be sustained. The first line of research attempts to embed robots with more human-like cognitive capabilities, and to create a new generation of assistance technology for both healthy and disabled people. Exoskeleton robots are an important area of application of this line (see e.g. [1, 2, 3, 4] for some of them designed for the upper limb). By contrast, the other line of research attempts to control already existing robots through human-friendly means. This includes ordinary robots which are employed for useful work, as well as the development of human interfaces for already existing robotics systems. The impact of this approach is expected to be important for example in nursing and patient aiding, in helping humans in surgery and other complex tasks in health care, and also in implementing space-restricted systems wherever alternative input-output devices are not flexible (refer to [5, 6, 7, 8] for some examples). This paper focuses on the second line of research.

There are two main reasons to develop surgical robots. On the one hand, they can improve the effectiveness of surgical procedures, applying available information with effectiveness, to perform a better action in the operating room. On the other hand, they can bring an improvement upon the physical limitations of a surgeon or a radiologist, all the while letting them control the procedure. That is why currently it is a surgeon who has direct control of a surgical robot. This is often done using teleoperation, i.e. the human operator manipulates an input device, and then a patient-side robot follows the input. Thus, the physical coupling between a human and a robot is a challenging task, so as to stably and naturally integrate the two systems. Capabilities for efficient robot interaction with humans can be found in [9, 10, 11, 12].

In what concerns human arm models, several papers have shown fractional derivatives to give the fractal nature of muscular tissue. For example, the dynamic behavior of muscles of different animal species (including humans) were modelled using fractional derivatives in [13, 14, 15, 16], and from a viscoelastic point of view in [17, 18]. In previous papers, it has been shown that fractional order transfer functions provide excellent models for a human arm [19, 20], both direct (relating the force at the hand, as input, with the arm angle, as output) and inverse (the other way round). In the current paper, such models are used to provide simulation results of how a KUKA LWR IV robot with 7 degrees of freedom (DOF) can be made to behave like a human arm. This means different things depending on whether control is

* Corresponding author e-mail: duarte.valerio@tecnico.ulisboa.pt

carried out in joint space or in Cartesian space. In the first case, each of the joints of the robot will behave like a human elbow. In the latter, all joints will behave in a manner which may not be that of an elbow, but so that the overall effect is that of the human arm. Our motivation results from surgical (e.g. orthopedic) applications.

The paper's contribution is to show that this is possible, and that a model with fractional derivatives is most suited for the purpose, and for its applications, namely in an operating theatre as mentioned above. There is thus a double motivation for this research. The principal motivation is to emulate the dynamics of a human arm by means of a 7-DOF KUKA LWR IV robot, using the previously obtained inverse model of the human arm. These results could not be obtained using only the control features provided with the robot. The second motivation is to demonstrate that the fractional dynamics of the human arm can be successfully used to simulate the control of the robot, and make it behave in a manner similar to that of a human arm during surgery.

The paper is organised as follows. Section 2 summarizes alternative models for the human arm. Section 3 presents the robot to be used. Sections 4 and 5 show the results of control in joint space and in Cartesian space. Comments and conclusions are drawn in Section 6.

2 Human arm models

As mentioned above, both direct and inverse models for the human arm, published in [19, 20], were obtained from data collected with the assistance of nine female and nine male volunteers, with ages ranging from 25 to 66, without any known musculo-skeletal injuries of the higher limbs. They kneeled or sat, holding a horizontal robotic arm, while trying to keep it steady. At the same time, the robotic arm, which was actuated by a Kollmorgen direct drive D061M-23-1310 motor, moved randomly. Experiments lasted 40 s to avoid fatigue, and were grouped into three types: (i) type I, oscillations in both directions around the zero-point; (ii) type II, oscillations only in the positive side of the zero-point (flexion of the elbow); and (iii) type III, oscillations only in the negative side of the zero-point (extension of the elbow).

Data was used to find transfer functions $G_{direct}(s) = \frac{\theta(s)}{F_{measured}(s)}$ and $G_{inverse}(s) = \frac{F_{measured}(s)}{\theta(s)}$, where θ is the measured arm angle, and $F_{measured}$ is the force at the hand, respectively. More details are given in this paper's Appendix. The model used in what follows is

$$G_{inverse}(s) = \frac{F_{measured}(s)}{\theta(s)} = \frac{1550.49(s^{1.52}+61.66)(s^{1.52}+605.19)}{s^{3.04}+1872.72s^{1.52}+1232403.37} \tag{1}$$
$$\approx \frac{1656.54(s+67)(s+38.8)(s+2.3)(s^2+13.8s+206.37)(s^2+68s+4889.21)}{(s+61.9)(s+15.5)(s+2.2)(s^2+120.6s+8820.09)(s^2+29.6+11433.85)}$$

This is a fractional order, linear, time-invariant model. Such models appear because the plant can be described with a differential equation involving fractional derivatives (about which interested readers may read more in [21, 22, 23, 24, 25, 27]). This fractional transfer function was then approximated by a 7th order integer transfer function as shown above.

3 The robot

The KUKA LWR IV+ is a 7-DOF (hence intrinsically redundant) robot, weighting 15 kg and handling a useful load of up to 7 kg (see Fig. 1). It is a low energy consumption robot designed for precision positioning and direct human interaction. The robot was controlled from a computer using the Fast Research Interface (FRI) system [26], communicating with the robot via UDP with a bandwidth in the [10 Hz, 1 kHz] range, and allowing real time access to measured and estimated signals. (Joint coordinates and joint torques are measured; the position and pose of the terminal element, and the applied forces and torques, are estimated.) Impedance control is used to control the robot, both in the joint space and in Cartesian space, causing a mass-spring-dashpot behaviour, which must then be controlled to achieve a human arm-like behaviour [26]. Readers interested in details about impedance control may find details e.g. in book [28].

3.1 Control in joint space

The control action $\boldsymbol{\tau}_{CMD}$ (which is a vector with values of control actions for each of the joints) is given by

$$\boldsymbol{\tau}_{CMD} = \boldsymbol{K}(\boldsymbol{\theta}_{ref} - \boldsymbol{\theta}) + D(\boldsymbol{\xi}, \dot{\boldsymbol{\theta}}) + \boldsymbol{\tau}_{user} + f_{dyn}(\boldsymbol{\theta}, \dot{\boldsymbol{\theta}}, \ddot{\boldsymbol{\theta}}) \tag{2}$$

where $\boldsymbol{K}$ is a diagonal matrix with the stiffness values desired for each joint, $\boldsymbol{\theta}_{ref}$ is a vector with the desired joint coordinates, $\boldsymbol{\theta}$ is a vector with the actual joint coordinates, $\boldsymbol{\xi}$ is a vector with the desired damping coefficients for each

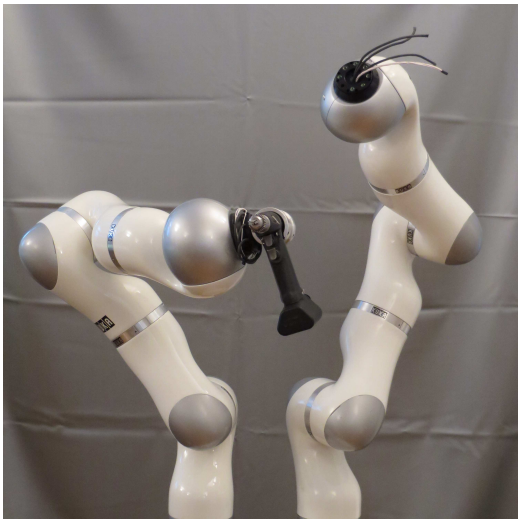

Fig. 1: The 7 degree of freedom KUKA LWR IV+ robot; this paper deals with one of the robotic arms only

joint, D is the damping of the control actions (being a function of the desired damping coefficients and of joint speeds), $\boldsymbol{\tau}_{user}$ is a vector with binaries freely chosen by the user, and f_{dyn} is a term with compensations for gravity, centrifugal and Coriolis forces acting on the robot's links. This term is calculated by KUKA's software [29]. This achieves for each joint a dynamical behaviour given by

$$\tau(t) = I_\theta \ddot{\theta} + D_\theta \dot{\theta} + K_\theta \left(\theta(t) - \theta_{ref}(t)\right) \tag{3}$$

$$I_\theta = \frac{K_\theta}{\omega_n^2} \tag{4}$$

$$D_\theta = \frac{2\xi_\theta K_\theta}{\omega_n} \tag{5}$$

where K_θ is the joint's stiffness, I_θ is the inertia, D_θ is the effective damping, ξ_θ is the damping factor, and ω_n is the natural frequency of the second order behaviour obtained by FRI. FRI allows setting for each joint K_θ and ω_n; ω_n cannot be set, but is chosen by FRI from K_θ and the robot's configuration.

Applying the Laplace transform to the above,

$$\Theta(s) = \frac{K_\theta}{I_\theta s^2 + D_\theta s + K_\theta}\Theta_{ref}(s) + \frac{1}{I_\theta s^2 + D_\theta s + K_\theta}\tau(s) \tag{6}$$

3.2 Control in Cartesian space

The control action $\boldsymbol{\tau}_{CMD}$ is now given by

$$\boldsymbol{\tau}_{CMD} = \mathscr{J}(\boldsymbol{\theta})^T \left(\boldsymbol{K}(\boldsymbol{x}_{ref} - \boldsymbol{x}) + D(\boldsymbol{\xi}, \dot{\boldsymbol{x}}) + \boldsymbol{F}_{user}\right) + f_{dyn}(\boldsymbol{\theta}, \dot{\boldsymbol{\theta}}, \ddot{\boldsymbol{\theta}}) \tag{7}$$

where $\boldsymbol{x}_{ref}$ is a vector with the desired pose (Cartesian coordinates of the manipulator and its orientation), $\boldsymbol{\theta}$ is a vector with the actual pose, $\boldsymbol{F}_{user}$ is a vector with forces freely chosen by the user, $\mathscr{J}(\boldsymbol{\theta})$ is the geometric Jacobian, and other variables are as in (2). The geometric Jacobian is given by

$$\mathscr{J}(\boldsymbol{\theta}) = \left[\mathscr{J}_{\boldsymbol{X}}(\boldsymbol{\theta}) \;\; \mathscr{J}_{\boldsymbol{\Phi}}(\boldsymbol{\theta})\right]^T \tag{8}$$

$$[\dot{x} \;\; \dot{y} \;\; \dot{z}]^T = \mathscr{J}_{\boldsymbol{X}}(\boldsymbol{\theta})\dot{\boldsymbol{\theta}} \tag{9}$$

$$[\omega_x \;\; \omega_y \;\; \omega_z]^T = \mathscr{J}_{\boldsymbol{\Phi}}(\boldsymbol{\theta})\dot{\boldsymbol{\theta}} \tag{10}$$

where x, y and z are the Cartesian coordinates of the terminal element, and ω_x, ω_y and ω_z are its rotation velocities. In other words, the geometric Jacobian relates the rotation of the joints with the pose of the terminal element.

The Laplace transform leads now to transfer function

$$X(s) = \frac{K_x}{M_x s^2 + D_x s + K_x} X_{ref}(s) + \frac{1}{M_x s^2 + D_x s + K_x} X(s) \tag{11}$$

which holds for each of coordinates x, y, z, ω_x, ω_y and ω_z. Variables are analogous to those of the joint space case; so are expressions for M_x and D_x similar to (4)–(5) for I_θ and D_θ.

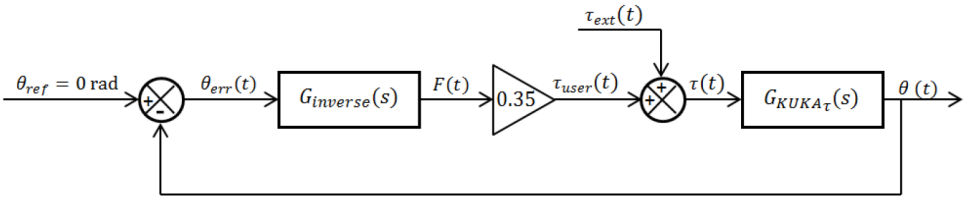

Fig. 2: Control in joint space: loop for one joint; symbols defined in text

4 Results of control in joint space

The purpose of control in joint space is to get each of the joints of the robot to behave like the elbow of a human arm, as modelled by (1). The control loop for each joint is shown in Fig. 2, where 0.35 m is the average length of the human upper arm, $\tau_{ext}(t)$ denotes the external perturbations applied to the joint, τ_{user} was defined in (2), and $G_{KUKA_\tau}(s)$ stands for the dynamics of the robot. Results are assessed by four performance indexes: mean squared error (MSE), mean absolute deviation (MAD), maximum deviation (MD) and variance accounted for (VAF). Letting y be the desired result and $\hat{y}$ the experimental result, they are given by:

$$MSE = \frac{\sum_{j=1}^{N} (y_j - \hat{y}_j)^2}{N} \tag{12}$$

$$MAD = \frac{\sum_{j=1}^{N} |y_j - \hat{y}_j|}{N} \tag{13}$$

$$MD = \max_N |y_j - \hat{y}_j| \tag{14}$$

$$VAF = 1 - \frac{\sigma^2(\mathbf{y} - \hat{\mathbf{y}})}{\sigma^2(\mathbf{y})} \tag{15}$$

(σ^2 denotes the variance.) In our case, the desired result is the position of the joint, measured in the plane of the two links it connects.

Three different manners of implementing control in joint space were tried:

- Natural frequencies ω_n were identified for the particular configuration of the robot seen in Fig. 3 (chosen because it is used during a particular orthopedic surgery currently under study [19]), with values of stiffness and damping for each joint set midway between the lower and higher values that FRI allows. It was expected that parameters would not change too much for other configurations, or that control would be able to compensate for that. But results obtained were poor (and are not shown).
- Values of stiffness and damping for each joint were set as low as the FRI allows, to obtain joints as complacent as possible. Control achieved much better results, but still not satisfactory; these too are not shown.
- Values of stiffness and damping for each joint were optimised to improve the performance measured by indexes (12)–(15), using a genetic algorithm [30]. This was the strategy that led to the best results, shown below.

The genetic algorithm was as follows:

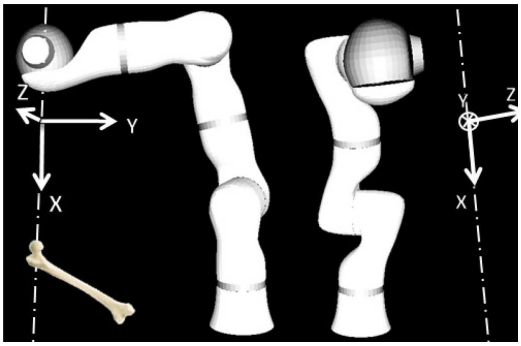

Fig. 3: Pose of the KUKA LWR IV+ robot used to identify the parameters of its dynamic behaviour; the bone is the patient's, in orthopedic surgery

–*Initial population:* 40 individuals are generated with random values for rigidity K, damping ξ and natural frequency ω_n.
–*Control performance:* this is assessed using the VAF (15) of the positioning error.
–*Natural selection:* the 20 worst performing individuals are eliminated.
–*Pairing:* the other 20 individuals are randomly paired.
–*Reproduction:* each pair generates two new individuals. One of the three variables is randomly selected; let it be Υ. The two descendants will have

$$\Upsilon_1 = \Upsilon_{father} + r(\Upsilon_{father} - \Upsilon_{mother}) \tag{16}$$
$$\Upsilon_2 = \Upsilon_{mother} - r(\Upsilon_{father} - \Upsilon_{mother}) \tag{17}$$

where $r \in [0,1]$ is a random number. As to the two other variables, one descendent will received one from the father and one the mother, and vice-versa for the other.
–*Mutation:* these 20 descendants have, in all, 60 variables, of which 12 are randomly selected, to be randomly replaced.
–*Convergence test:* at least 20 generations are created. From then on, if any time there has be an improvement in the VAF of less than 0.1% over the last 6 generations, the algorithm stops.

Parameters and performances obtained are given in Table 1. Figure 4 shows part of the response of the model of the human arm to a random solicitation (as used during the identification process) and compares this with the response the robot achieves with control in joint space. The two responses are seen to be close, as expected from the low values of the indexes in Table 1.

Table 1: Parameters and performances of control in joint space, for each one of the joints

Stiffness	34.19	Nm/rad
Damping	0.43	
Natural frequency	26.65	rad/s
MSE	2.444×10^{-5}	rad^2
MAD	3.461×10^{-3}	rad
MD	1.784×10^{-2}	rad
VAR	40.07	%

Still using control in joint space, when there is a trajectory reference in Cartesian space, control is achieved as seen in Fig. 5. In this block diagram, account is taken that during a surgical operation the patient may move, and so the direction which the robot ought to follow changes in an inertial referential. Performance is checked, not with a perturbation applied in each joint in the plane of the links that the joint connects, but rather with a perturbation applied at the terminal element of the robot, in a plane perpendicular to the axis shown in Fig. 3. In that plane, there are many possible directions; let β be the angle that defines the direction in the plane, and $\beta = 0^\circ$ the direction pointing to the first joint. Stiffness and damping coefficients had to be recalculated for every single joint depending on β. Values and performances are given in Table

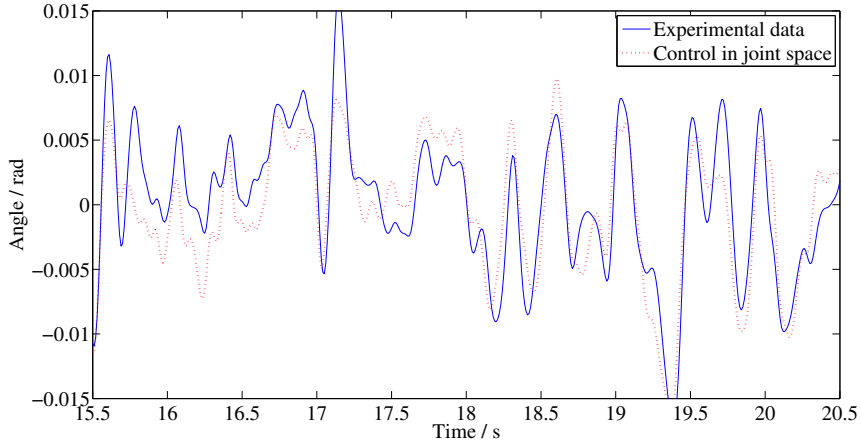

Fig. 4: Performance of control in joint space, corresponding to Table 1

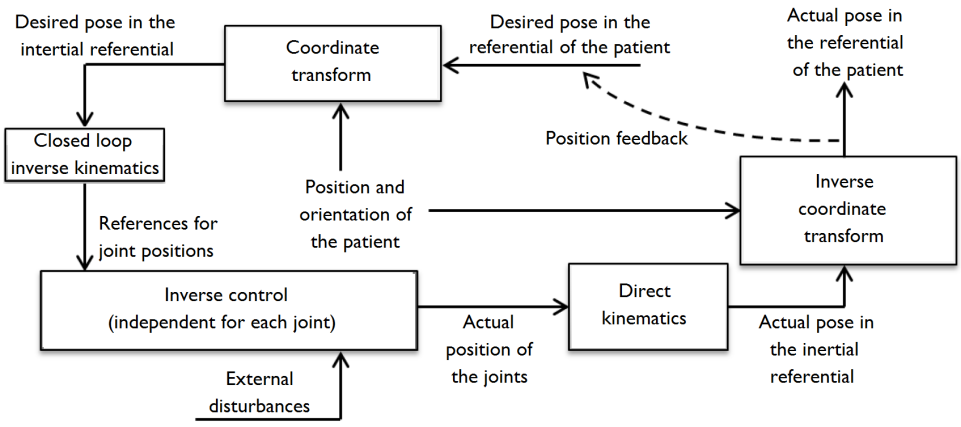

Fig. 5: From joint control to control in the Cartesian space

2 for the first joint. Results are similar for most other joints, save for those with rotation axes in the same plane of the perturbation, which can do little to cope with it. This shows why for this type of perturbations it is better to use control in Cartesian space rather than the control strategy of Fig. 5. Indeed, since we do not know the direction of the perturbation, it would have to be estimated by the FRI in each instant, and the control parameters would have to be time-varying. Consequently, this approach would be very sensitive to any mistake in FRI estimations.

Table 2: Parameters for the first joint and performances of control in joint space, with a perturbation applied to the terminal element of the robot

β / °	Stiffness / Nm/rad	Damping	Natural frequency / rad/s	MSE / mm^2	MAD / mm	MD / mm	VAF / %
0	126.18	0.496	23.77	1.836	1.099	6.011	18.87
30	91.08	0.499	24.01	1.743	1.245	5.749	24.10
60	39.80	0.497	25.21	1.933	1.331	6.105	31.26
90	147.25	0.435	25.33	2.021	1.224	5.928	17.62
120	342.28	0.563	23.16	1.581	1.132	5.536	36.07
150	167.78	0.524	23.44	1.461	1.083	5.339	34.66

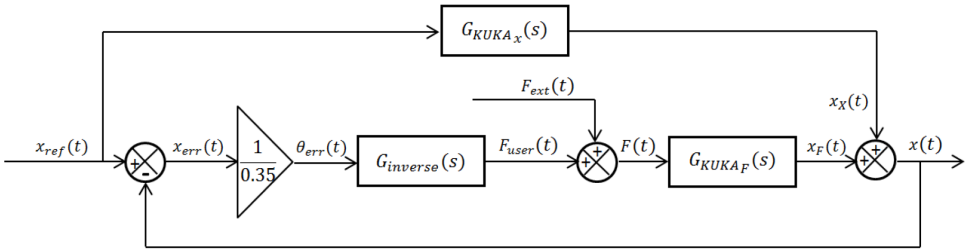

Fig. 6: Control in Cartesian space: loop for one joint; symbols defined in text

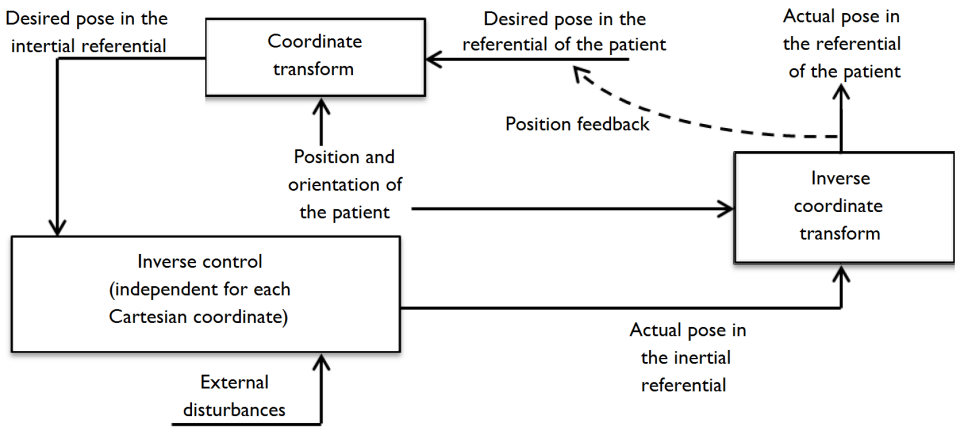

Fig. 7: Control in the Cartesian space (cf. Fig. 5)

5 Results of control in Cartesian space

When working in Cartesian space, the control loop is shown in Fig. 6, where $G_{KUKA_x}(s)$ is a term that reflects the changes in the operating point of the robot in Cartesian space. Results are assessed as before. The diagram of Fig. 5 is replaced by that in Fig. 7, which is simpler.

For each direction, the stiffness, the damping factor and the natural frequency were optimised as above. Results for different values of β are given in Table 3 and can be seen to be rather constant. So average values can be used, irrespective of the direction of the perturbation in the plane perpendicular to the axis where the robot is moving, leading to the performances recorded in Table 4. It is clear that errors are almost always far lower (and the VAF higher) in 4 than in Table 2, proving the superiority of control in Cartesian space. Parts of the simulations are shown (for one particular value of β) in Figs. 8 (for each Cartesian direction separately) and 9 (now measured in the direction of the perturbation). In all cases the robot reproduces the desired movement.

Table 3: Parameters for control in Cartesian space, with a perturbation applied to the terminal element of the robot

	Stiffness / Nm/rad			Damping			Natural frequency / rad/s		
β / °	Ox	Oy	Oz	Ox	Oy	Oz	Ox	Oy	Oz
0	296.70	294.61	294.78	0.39	0.39	0.39	26.31	26.42	26.26
30	282.45	294.68	297.68	0.41	0.41	0.38	25.95	26.38	26.51
60	286.57	295.40	289.70	0.42	0.38	0.42	26.74	26.61	26.13
90	303.29	300.29	296.64	0.39	0.39	0.40	26.87	26.56	26.55
120	289.33	289.02	288.71	0.41	0.40	0.41	26.36	26.48	26.82
150	299.13	299.61	288.02	0.38	0.41	0.43	26.41	26.53	26.60
Averages		293.70			0.40			26.47	

Table 4: Performances of control in Cartesian space, with a perturbation applied to the terminal element of the robot, using the average parameters of Table 3

	MSE / mm^2			MAD / mm			MD / mm			VAF / %		
β / °	Ox	Oy	Oz	Ox	Oy	Oz	Ox	Oy	Oz	Ox	Oy	Oz
0	0.00005	2.955	0.041	0.003	1.203	0.142	0.014	6.207	0.931	40.10	40.10	40.10
30	0.741	2.241	0.015	0.602	1.048	0.087	3.103	5.404	0.449	40.08	40.09	40.10
60	2.232	0.762	0.0002	1.046	0.611	0.009	5.395	3.155	0.046	40.09	40.10	40.08
90	2.985	0.0002	0.010	1.209	0.011	0.071	6.545	0.058	0.0369	40.08	40.09	40.10
120	2.245	0.715	0.036	1.049	0.592	0.133	5.408	3.053	0.685	40.10	40.10	40.09
150	0.752	2.194	0.051	0.607	1.036	0.158	3.133	5.348	0.817	40.10	40.09	40.09
Averages	1.493	1.478	0.026	0.753	0.750	0.100	3.883	3.870	0.516	40.10	40.10	40.10

6 Conclusions

We could think that it should suffice to use the optimisation above to find impedance control parameters ensuring a behaviour as close as possible to that of the human arm, without resorting to the control loop of Fig. 2. This is indeed possible, as shown in Fig. 10: the two curves are indistinguishable. But since the natural frequency is not known and can indeed vary, this is not a good idea, because results are not robust to changes in the natural frequency, as shown in Fig. 11. Of course, we do not want our control to deteriorate in this way. What this means is that the control scheme of Fig. 6 is unavoidable.

We conclude that the models obtained when identifying the dynamics of the human arm can be successfully used to simulate the control the KUKA LWR IV+ robot, and make it behave in a manner similar to that of a human arm, when performing surgery. These results could not be obtained using only the control features provided with the robot.

Future work includes developing ways of providing robustness to variations in the mass of the surgical tool the robot is holding, and, of course, extensive experimental tests of these results.

Acknowledgement

This work was supported by FCT, through IDMEC, under LAETA, project UID/EMS/50022/2019.

Appendix: More about models of the human arm

Third order integer linear models. These models are often employed for this system in the literature (see e.g. [31]), both because experimental data can be reasonably fitted, and because there is a clear analogy shown in Fig. 12. Identification methods applied were the same given below for fractional transfer functions (restricting differentiation orders to integers, of course). The best results were obtained for models with three poles and one zero for direct arm dynamics, and with three poles for the inverse case.

Fractional linear models. A measured time response can be directly used to identify a fractional transfer function [32, 27], but in this case it was preferred to first identify a frequency response (using Welch's method on the filtered output), and then apply Levy's method. This alternative leads to less noisy results. Levy's method takes a frequency response $G(j\omega_p),\ p = 1,\ldots,f$ and fits thereto a commensurable fractional model, the frequency response of which is given by

$$\hat{G}(j\omega_p) = \frac{\sum_{k=0}^{m} b_k (j\omega_p)^{k\alpha}}{1 + \sum_{k=1}^{n} a_k (j\omega_p)^{k\alpha}} = \frac{N(j\omega_p)}{D(j\omega_p)} \tag{18}$$

Levy's method minimizes $(G(j\omega)D(j\omega) - N(j\omega))^2$. The commensurable orders of fractional models were found sweeping all values $\alpha = 0, 0.1, 0.2, \ldots, 1.9, 2]$ (outside this range, no transfer function is stable). Then the α for which results are better, using a heuristic based on some performance indexes, was kept. In this case, the best direct arm model had two poles and one zero and two poles in the inverse case.

Comparing performances. Time responses and frequency responses of these models, and also of neural network models, were compared for inputs of all types (I, II and III). The performance of fractional models was superior, while needing less parameters. For more details see [20].

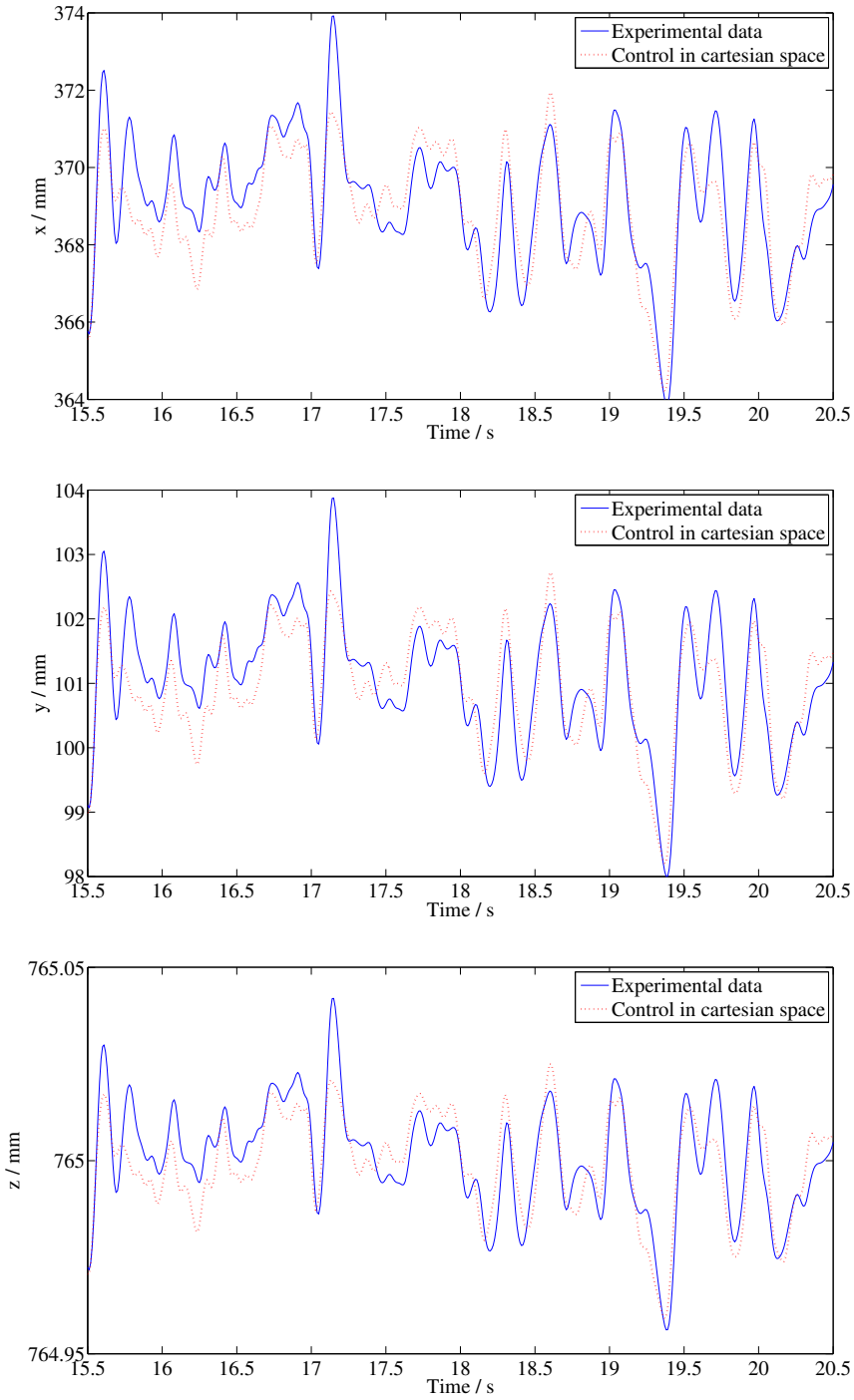

Fig. 8: Performance of control in Cartesian space, corresponding to $\beta = 60^\circ$ in Table 4, according to directions Ox (a), Oy (b) and Oz (c)

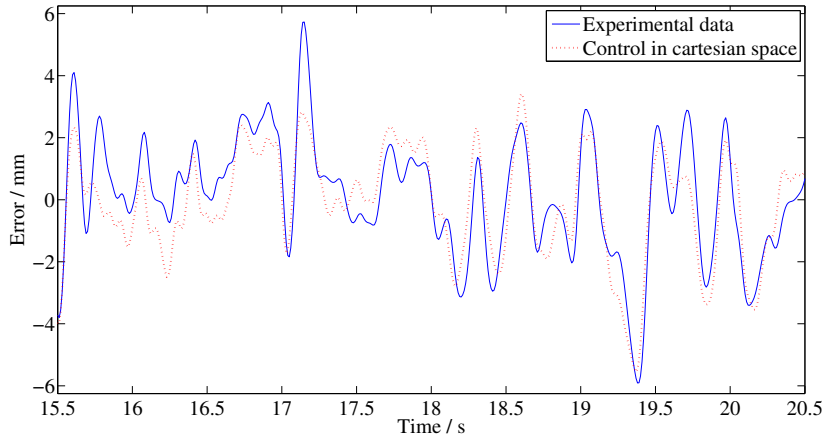

Fig. 9: Performance of control in Cartesian space, as in Fig. 8, according to the direction of the perturbation

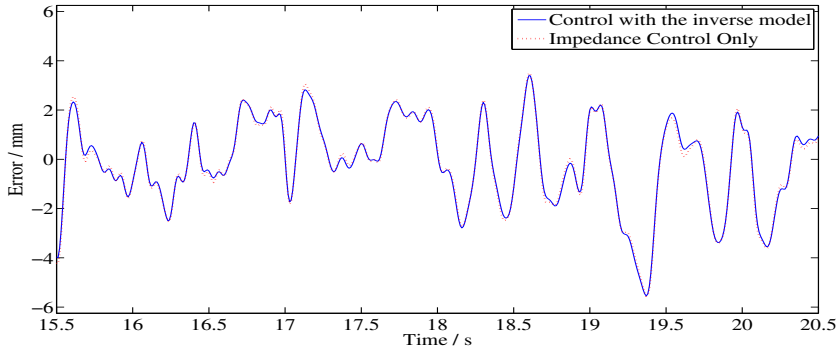

Fig. 10: Performance comparison of the robot with impedance control alone and with the loop of Fig. 2, for nominal values of the natural frequency

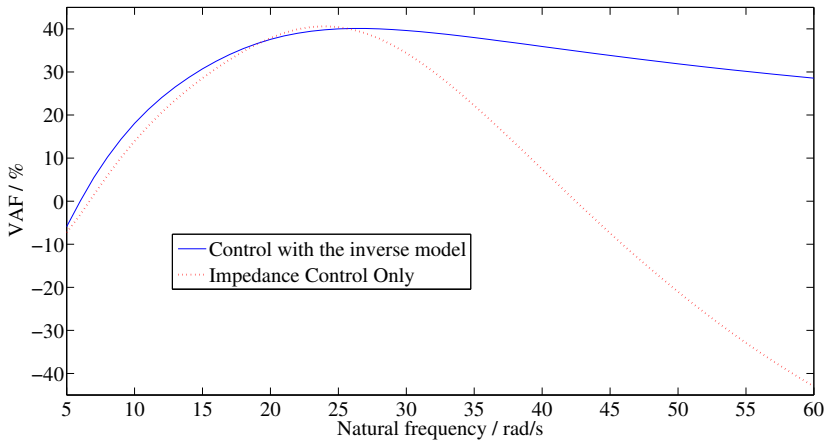

Fig. 11: Performance comparison of the robot with impedance control alone and with the loop of Fig. 2, when the natural frequency changes

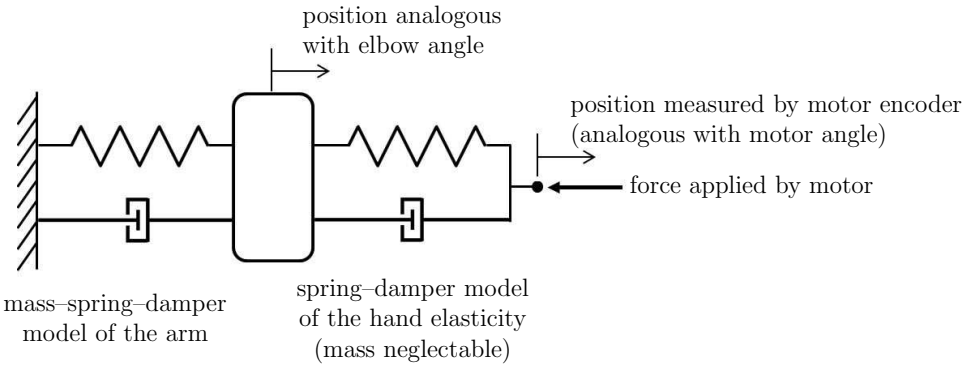

Fig. 12: Third order translation analog to elbow dynamics

References

[1] N. Jarrassé, T. Proietti, V. Crocher, J. Robertson, A. Sahbani, G. Morel and A. Roby-Brami, Robotic exoskeletons: A perspective for the rehabilitation of arm coordination in stroke patients. *Front. Hum. Neurosci.* **8**, 1–13 (2014).
[2] H. Kim, L. M. Miller, N. Byl, G. M. Abrams and J. Rosen, Redundancy resolution of the human arm and an upper limb exoskeleton, *IEEE Transact. Biomed. Eng.* **59**(6), 1770–1778 (2012).
[3] H. S. Lo and S. Q. Xie, Exoskeleton robots for upper-limb rehabilitation: State of the art and future prospects, *Med. Eng. Phys.* **34**(3), 261–268 (2012).
[4] J. Rosen, J. C. Perry, N. Manning, S. Burns and B. Hannaford, The human arm kinematics and dynamics during daily activities—toward a 7 dof upper limb powered exoskeleton, In *Proceedings of the 12th international conference on advanced robotics (ICAR'05)*, 532-539 (2005).
[5] S. E. Butner and M. Ghodoussi, Transforming a surgical robot for human telesurgery, *IEEE Transact. Robotic. Aut.* **19**(5), 818–824 (2003).
[6] H. Mayer, F. Gomez, D. Wierstra, I. Nagy, A. Knoll and J. Schmidhuber, A system for robotic heart surgery that learns to tie knots using recurrent neural networks, *Adv. Robot*, **22**(13-14), 1521–1537 (2008).
[7] R. Muradore, D. Bresolin, L. Geretti, P. Fiorini and T. Villa, Robotic surgery, *IEEE Robot. Automat. Mag.* **18**(3), 24–32 (2011).
[8] J. Rosen, B. Hannaford and R. M. Satava, editors, *Surgical robotics. Systems applications and vision*, Springer, 2011.
[9] N. Jarrassé, V. Sanguineti and E. Burdet, Slaves no longer: Review on role assignment for human-robot joint motor action, *Adapt. Behav.* **22**(1), 70–82 (2014).
[10] S. Park, H. Lim, B.-S. Kim and J.-B. Song, Development of safe mechanism for surgical robots using equilibrium point control method, In Rasmus Larsen, Mads Nielsen, and Jon Sporring, editors, *Medical image computing and computer-assisted intervention — MICCAI 2006*, volume 4190 of Lecture Notes in Computer Science, pp. 570–577, Springer Berlin / Heidelberg, 2006.
[11] V. Potkonjak, S. Tzafestas, D. Kostic and G. Djordjevic, Human-like behavior of robot arms: General considerations and the handwriting task — Part I: Mathematical description of human-like motion: distributed positioning and virtual fatigue, *Robot. Comput. Integ.Manufact.* **17**(4), 305–315 (2001).
[12] K. Sakita, K. Ogawara, S.Murakami, K. Kawamura and K. Ikeuchi, Flexible cooperation between human and robot by interpreting human intention from gaze information. In *Proceedings the 2004 IEEE/RSJ International conference on intelligent robots and systems (IROS2004)*, pp. 846851 (2004).
[13] V. D. Djordjevic, J. Jaric, B. Fabry, J. J. Fredberg and D. Stamenovic, Fractional derivatives embody essential features of cell rheological behavior, *Annals Biomed. Eng.* **31**:692-699, (2003).
[14] L. Sommacal, P. Melchior, J.-M. Cabelguen, A. Oustaloup and A. J. Ijspeert, *Advances in Fractional Calculus: Theoretical Developments and Applications in Physics and Engineering*, chapter *Fractional Multimodels of the Gastrocnemius Muscle for Tetanus Pattern*, pp. 271–285, Springer-Verlag, 2007.
[15] L. Sommacal, P. Melchior, A. Dossat, J. Petit, J.-M. Cabelguen, A. Oustaloup and A. J. Ijspeert, Improvement of the muscle fractional multimodel for low-rate stimulation, *Biomed. Sign. Proc. Contr.* **2** 226–233 (2007).
[16] L. Sommacal, P. Melchior, A. Oustaloup, J.-M. Cabelguen and A. J. Ijspeert, Fractional multi-models of the frog gastrocnemius muscle, *J. Vibr. Contr.* **14**(9-10), 1415–1430 (2008).
[17] R. L. Magin, *Fractional calculus in bioengineering*, Begell House, 2004.

[18] F. Mainardi, *Fractional calculus and waves in linear viscoelasticity, An introduction to mathematical models*, Imperial College Press, London, 2010.
[19] I. Tejado, D. Valério, P. Pires and J. Martins, Fractional order human arm dynamics with variability analyses, *Mechatronics* **23**, 805–812 (2013).
[20] A. Ventura, I. Tejado, D. Valério and J. Martins, Fractional direct and inverse models of the dynamics of a human arm, *J. Vibr. Contr.* **22**(9), 2240–2254 (2016).
[21] K. S. Miller and B. Ross, *An introduction to the fractional calculus and fractional differential equations*, John Wiley and Sons, New York, 1993.
[22] C. A. Monje, Y. Q. Chen, B. M. Vinagre, D. Xue and V. Feliu. *Fractional-order systems and controls. Fundamentals and applications*, Springer, 2010.
[23] I. Podlubny, *Fractional differential equations: An introduction to fractional derivatives, fractional differential equations, to methods of their solution and some of their applications*, Academic Press, San Diego, 1999.
[24] S. G. Samko, A. A. Kilbas and O. I. Marichev, *Fractional integrals and derivatives*, Gordon and Breach, Yverdon, 1993.
[25] D. Valério and J. S. da Costa, An introduction to single-input, single-output Fractional Control. *IET Control Theory & Applications*, **5**(8):1033-1057, 2011.
[26] G. Schreiber, A. Stemmer and R. Bischoff, The fast research interface for the KUKA lightweight, In *Proceedings of the IEEE International Conference on Robotics and Automation*, 2010.
[27] D. Valério and J. S. da Costa, *An introduction to fractional control* IET, 2013. , ISBN 978-1-84919-545-4.
[28] B. Siciliano, L. Sciavicco, L. Villano and G. Oriolo, *Robotics — Modelling, Planning and Control*, Springer, 2009.
[29] A. Albu-Schäffer and Gerd Hirzinger, Cartesian impedance control techniques for torque controlled light-weight robots. In *IEEE International Conference of Robotics and Automation*, pages 657-663, Washington DC, 2002.
[30] J.-S. R. Jang, C.-T. Sun, and E. Mizutani, *Neuro-fuzzy and soft computing*, Prentice-Hall, Upper Saddle River, chapters 8 to 11 (1997).
[31] M. J. Fu and M. C. Cavusoglu, Human-arm-and-hand-dynamic model with variability analyses for a stylus-based haptic interface, *IEEE Transact. Syst. Man Cyber. B: Cyber.* **42**(6), 1633–1644 (2012).
[32] R. Malti, S. Victor and A. Oustaloup, Advances in system identification using fractional models, *ASME J. Comput. Nonlin. Dynam.* **3**, 021401 (2008).